PHYSICAL REVIEW B

CONDENSED MATTER

THIRD SERIES, VOLUME 48, NUMBER 15 15 OCTOBER 1993-I

Valence-bond analysis of half-filled dimerized Hubbard chains

Anna Painelli and Alberto Girlando

Istituto di Chimica Fisica, Università di Parma, Via delle Scienze, 43100 Parma, Italy

(Received 30 November 1992; revised manuscript received 17 June 1993)

The diagrammatic valence-bond technique is adopted to investigate one-dimensional half-filled Hubbard chains with long-range *e*-*e* interactions and alternating charge-transfer integrals. Exact results for finite-size systems with different boundary conditions are carefully extrapolated to the infinite-chain limit. In addition to various ground-state properties, such as bond-charge-density wave and bond-order amplitude, we calculate the optical gap and the corresponding oscillator strength. We introduce adiabatic phonons able to modulate on-site energies and investigate the stability of the system with respect to site-charge-density wave distortion. We also evaluate the response of the electronic system to the perturbation induced by adiabatic phonons which modulate charge-transfer integrals, and calculate the corresponding screening of vibrational frequencies.

I. INTRODUCTION

One-dimensional (1D) Hubbard chains with alternating charge-transfer (CT) integrals have been extensively studied[1,2] in the past few years as model systems for conjugated polymers such as polyacetylene. The alternation of CT integrals originates from the dimerization of the underlying chain and is driven by phonons which modulate CT integrals (bond-diagonal electron-phonon (*e*-ph) coupling). The amplitude of the resulting bond-charge density wave (bond-CDW) and its dependence on the on-site and intersite electron-electron (*e*-*e*) interactions have been the focus of many papers.[1-15] On the other hand, the same model is also relevant to a second class of compounds, i.e., half-filled segregated stack CT salts such as K-TCNQ.[16] In these systems, as well as in conjugated polymers with complex structure, electrons also couple to phonons that modulate on-site energies (site-diagonal *e*-ph coupling). This coupling favors a site-CDW distortion, and the actual ground-state structure of the system is determined by the interplay between bond- and site-diagonal *e*-ph coupling and on-site and intersite *e*-*e* interactions.[17-20]

In this paper we present the results of extensive diagrammatic valence-band (DVB) calculations[21] on half-filled 1D Hubbard chains with different strengths of on-site and intersite long-range *e*-*e* interactions, and variable CT integral alternation. In particular, we calculate ground-state properties such as energy, bond-order, and bond-CDW amplitude for rings with periodic or antiperiodic boundary conditions. In the adiabatic approximation we also calculate phonon susceptibilities, i.e., the electronic response to site- and bond-diagonal *e*-ph perturbation.[17-19] The finite-size results are carefully extrapolated to the infinite-chain limit. Whereas the dependence of the bond-CDW amplitude on the bond-diagonal *e*-ph coupling strength and on the strength of on-site and intersite *e*-*e* interactions compares well with the results of the most recent calculations, we are also able to evaluate other properties of the system such as the optical gap and the total oscillator strength, or the perturbation of phonon frequencies due to *e*-ph coupling and the stability of the system with respect to site-CDW formation. Finally, in a subsequent paper[20,22] we will show how these results, together with those already obtained on systems with alternating on-site energies,[19] yield the complete phase diagram of the half-filled 1D chain in the presence of on-site and long-range intersite *e*-*e* interactions and on-site and on-bond *e*-ph coupling.

The paper is organized as follows: In Sec. II we present the Hamiltonian and the diagonalization procedure. In Sec. III we discuss the results of calculations performed in the absence of intersite *e*-*e* interactions. In Sec. IV we extend the calculation to account for intersite *e*-*e* interactions. Finite U results are compared with the $U=0$ ones; the analytical solution of the corresponding problem is sketched in the Appendix.

II. MODEL HAMILTONIAN

The long-range extended Hubbard Hamiltonian for a dimerized chain is written as

$$\mathcal{H}=2t\sum_i b_i-2t\varphi\sum_i(-1)^i b_i + U\sum_i a^{\dagger}_{i,\alpha}a^{\dagger}_{i,\beta}a_{i,\beta}a_{i,\alpha}+\sum_{i>j}V_{i,j}q_i q_j\ , \tag{1}$$

where

$$b_i=\sum_\sigma (a^\dagger_{i,\sigma}a_{i+1,\sigma}+\text{H.c.})/2$$

is the bond-order operator; $a^\dagger_{i,\sigma}$ ($a_{i,\sigma}$) is the creation (annihilation) operator for electrons with spin σ on site i; and $q_i=z_i-n_i$ is the charge operator for the site i, z_i being the charge of the vacuum site and n_i the electron number operator. The chain has alternating CT integrals, t' and t'': The mean CT integral is defined by $t=(t'+t'')/2$, and the alternation parameter is $\varphi=(t'-t'')/2t$. U measures the repulsion of two electrons on the same site, and $V_{i,j}$ the repulsion between two electrons on sites i and j. We consider an unscreened e-e potential: $V_{i,j}=V/r_{i,j}$, where $r_{i,j}$ is the distance between i and j sites and $V=V_{i,i+1}$. In this hypothesis the generalized Madelung constant α is $2\ln 2$ for the infinite chain (if only nearest-neighbor interactions are included, $\alpha=2$, whereas for a Pariser-Parr-Pople–Ohno parametrization,[1] $\alpha=1.25$). In the following the strength of intersite e-e interactions is measured by $\varepsilon_c=V(\alpha-1)$, and we put $\sqrt{2}|t|=1$.

We consider the coupling of the electron with adiabatic phonons modulating either on-site or on-bond energies. The corresponding e-mv and e-$l$ph Hamiltonians are ($\hbar=1$)[19]

$$\mathcal{H}_{e\text{-}mv}=N^{-1/2}\sum_\mu Q_\mu g_\mu\sqrt{\omega_\mu}\sum_i(-1)^i n_i\ , \tag{2a}$$

$$\mathcal{H}_{e\text{-}l\text{ph}}=N^{-1/2}\sum_\nu U_\nu g_\nu\sqrt{\omega_\nu}\sum_i(-1)^i b_i\ , \tag{2b}$$

where Q_μ and U_ν are the zone-center coordinates of on-site and on-bond phonons, $\omega_{\mu/\nu}$ and $g_{\mu/\nu}$ being the corresponding frequencies and e-ph coupling constants, respectively. The strength of the on-site and on-bond e-ph couplings is measured by the small polaron binding energy, $\varepsilon_{sp}=\sum_\mu g^2_\mu/\omega_\mu$ and by the lattice distortion energy $\varepsilon_d=\sum_\nu g^2_\nu/\omega_n$, respectively. In the adiabatic approximation the phonon Hamiltonians are

$$\mathcal{H}_{mv}=\tfrac{1}{2}\sum_\mu \omega^2_\mu Q^2_\mu\ , \tag{3a}$$

$$\mathcal{H}_{l\text{ph}}=\tfrac{1}{2}\sum_\nu \omega^2_\nu Q^2_\nu\ . \tag{3b}$$

Phonons modulating on-site energies break the electron hole and the reflection symmetry of the Hamiltonian in Eq. (1), whereas on-bond phonons are totally symmetric. In the adiabatic approximation the bond-diagonal coupling plays the same role as the alternation of CT integrals and, in fact, in this approximation, the bond-diagonal e-ph Hamiltonian in Eq. (2b) becomes[23]

$$\mathcal{H}_{e\text{-}l\text{ph}}=-4\varepsilon_d\beta\sum_i(-1)^i b_i\ , \tag{4}$$

where

$$\beta=\left\langle\sum_i(-1)^i b_i\right\rangle\Big/N$$

is the ground-state expectation value of the bond-CDW amplitude. If one assumes that the alternation of CT integrals is only due to the relaxation of bond-diagonal coupled modes, then, by comparing Eq. (1) with Eq. (4),

$$\varphi=\varepsilon_d\beta(2)^{3/2}\ . \tag{5}$$

Therefore, once the electronic Hamiltonian (1) is solved, from the $\beta(\varphi)$ curves one can extract the corresponding ε_d value, getting information on the e-ph coupled system. Moreover, the Herzberg-Teller approach to e-ph coupling[24] leads to the definition of two different phonon susceptibilities χ_v and χ_b, which describe the electronic response to on-site and on-bond e-ph perturbation:

$$\chi_v=\frac{2}{N}\sum_F\frac{\left|\langle G|\sum_i(-1)^i n_i|F\rangle\right|^2}{E_F-E_G}\ , \tag{6a}$$

$$\chi_b=\frac{8}{N}\sum_F\frac{\left|\langle G|\sum_i(-1)^i b_i|F\rangle\right|^2}{E_F-E_G}\ , \tag{6b}$$

where $|G\rangle$ and $|F\rangle$ represent the ground and an excited state of the electronic Hamiltonian, and E_G,E_F are the corresponding energies. The on-bond phonon susceptibility is simply related to the second derivative of the ground-state energy:

$$\chi_b=-2\frac{\partial^2 E_G}{\partial\varphi^2}=2\sqrt{2}\frac{\partial\beta}{\partial\varphi}\ . \tag{7}$$

The stability conditions with respect to Q_μ and U_ν relaxations are[23]

$$\varepsilon_{sp}<\chi_v^{-1}\ ,\qquad \varepsilon_d<\chi_b^{-1}\ . \tag{8}$$

Since χ_v and χ_b are purely electronic quantities, the effect of e-ph perturbations on the system can be investigated once a solution of the electronic problem is given.

The DVB technique,[21] which fully exploits spin-exchange symmetry, is an efficient approach to the diagonalization of Hubbard Hamiltonians for finite-size systems. We perform calculations on finite rings with periodic or antiperiodic boundary conditions. Periodic rings belong to the $C_{(N/2),v}$ point group, showing both rotational symmetry, i.e., the translational symmetry of the infinite chain, and reflection symmetry. For these systems we only investigate A_1 and A_2 subspaces, which in the infinite-chain limit correspond to the zero-wave vector states, which are symmetric (A_1) and antisymmetric (A_2) with respect to reflection. In antiperiodic rings the translational symmetry is lost, but symmetric and antisymmetric states are still distinguished with respect to reflection. Moreover, both periodic and antiperiodic rings show electron-hole symmetry: g and u states are defined as symmetric and antisymmetric with respect to electron-hole exchange. The ground state is found in the A_{1g} subspace for $N=4n$ rings, whereas it is in the A_{1u} subspace for $N=4n+2$ rings.

The exploitation of spin-exchange, electron-hole, and spatial symmetry allows us to diagonalize exactly the electronic Hamiltonian in Eq. (1) for rings up to ten sites on a VAX 3100 station. Infinite-chain results are ob-

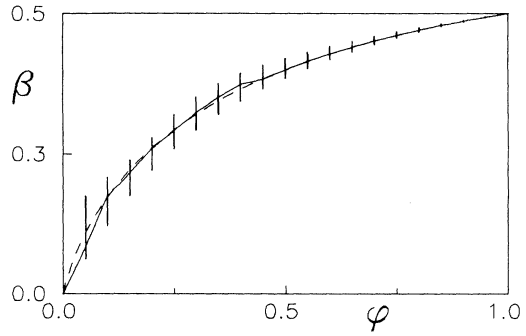

FIG. 1. The bond-CDW amplitude β as a function of φ for the infinite chain. The dashed curve refers to the analytical result, while the solid line shows the results of the extrapolation on periodic and antiperiodic finite systems with $N \leq 10$.

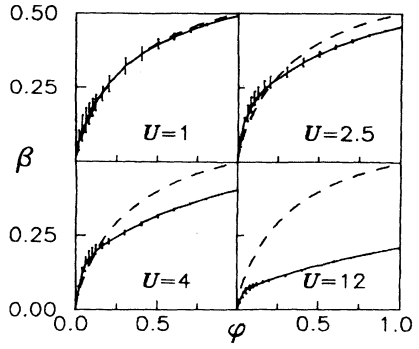

FIG. 2. The bond-CDW amplitude β as a function of φ for the infinite chain. The dashed lines refer to the noninteracting case.

tained by extrapolating data obtained with modified periodic boundary conditions (MPBC; periodic boundary conditions are assumed for $4n$ rings and antiperiodic ones for $4n+2$ rings) and with modified antiperiodic boundary conditions (MABC; antiperiodic boundary conditions are assumed for $4n$ rings and periodic ones for $4n+2$ rings).[12] In particular, unless stated differently, MPBC and MABC results for rings up to ten sites are interpolated (using the Marquardt algorithm[25]) with two polynomials, $y=c+d/N^i+f/N^j$, forced to the same c value, while i and j are integers between 1 and 4. The results obtained with the different i and j choices are then mediated, whereas the lowest and highest c values give an estimate of the uncertainty in the extrapolated results.

In order to gain confidence in the extrapolation procedure, we have tested it for the noninteracting ($U=0$) case, where exact results for the infinite chain are available. As an example, in Fig. 1 we compare the $\beta(\varphi)$ curve calculated for the noninteracting infinite chain (dashed line) with the extrapolated results. The agreement between the two curves is excellent, also considering that finite-size extrapolations are particularly difficult for noninteracting systems.

III. SYSTEMS WITH NO INTERSITE *e-e* INTERACTIONS ($V=0$)

In Fig. 2 we report, for different U, the φ dependence of the bond-CDW amplitude β. For $U=12$, the amplitude of the bond CDW is always lower than in the $U=0$ case (the dashed lines in the figure). On the contrary, for both $U=4$ and 2.5, there is a region where, for small φ, β is larger than in the noninteracting case (the uncertainties in the extrapolated results are too large to make any definite statement in the $U=1$ case). In other words, depending on the φ value, the $\beta(U)$ function either shows a maximum at intermediate U values or displays a strictly monotonous behavior. This behavior is strongly reminiscent of the U dependence of the dimerization amplitude (φ) as recently calculated[6,7,9–14] for various strengths of bond-diagonal *e*-ph coupling. The two results are indeed strictly related, since Eq. (5) allows us to extract from the $\beta(\varphi)$ curves the corresponding ε_d values. In Fig. 3 we report the bond-CDW amplitude (β) as a function of ε_d. This figure clearly shows the dimerization enhancement at small ε_d and intermediate U values. Our results are in quantitative agreement with previous partial results by Hirsch,[6] Hayden and Soos,[11] and Waas, Büttner, and Voit.[12]

We notice that, due to the φ dependence of β, φ and ε_d are not simply proportional [see Eq. (5)] and that, even if the information given in Fig. 3 is already implied in Fig. 2, the curves in Fig. 3 offer a more immediate picture of the physics of *e*-ph coupled systems. In particular, whereas β rapidly increases with φ near $\varphi=0$, the $\beta(\varepsilon_d)$ curves show a maximum slope at finite ε_d values. The divergence of

$$\frac{\partial\beta}{\partial\varepsilon_d}=2\sqrt{2}\frac{\partial\beta}{\partial\varphi}\left[1-(\varphi/\beta)\frac{\partial\beta}{\partial\varphi}\right]^{-1}$$

at $\varphi/\beta=(\partial\beta/\partial\varphi)^{-1}$, or $\varepsilon_d=\chi_b^{-1}$ [see Eqs. (5) and (7)] accounts for the sudden increase of β at finite ε_d values, which is clearly observed at large U, as well as for $U=0$. The physical origin of this behavior can be understood by realizing that whereas the regular chain is unstable with respect to dimerization, for each U a finite ε_d is required to obtain a non-negligible bond-CDW amplitude.

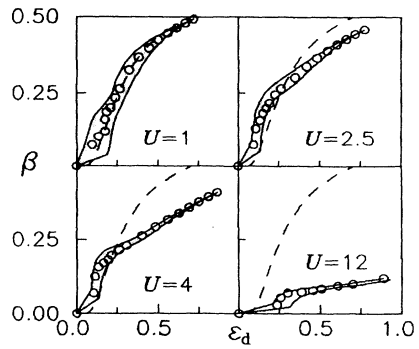

FIG. 3. The bond-CDW amplitude β as a function of φ for the infinite chain. The shaded regions correspond to the uncertainties in the extrapolated results (circles) for finite U. The dashed lines refer to the noninteracting case.

The mean bond order in the ground state, $b = \langle \sum_i b_i \rangle / N$, is a measure of the delocalization of the electrons along the chain. Moreover, together with β, it determines the total oscillator strength of the CT excitations,[26] $f_{CT} = \sqrt{2}(b + \varphi\beta)$. This quantity is particularly important since it is experimentally accessible and provides a useful check in the calculation of optical spectra, where the large finite-size dependence of the Drude contribution[27] can easily yield to incorrect interpretations. In Fig. 4 we present both the $\beta(\varphi)$ and the $f_{CT}(\varphi)$ curves calculated for different U values. Apart from a few b values presented in Ref. 28 for a $N=8$ system, as far as we know this is the first reported calculation of b, and then of f_{CT}, for chains with finite U and φ. The $\varphi=0$ (no bond-CDW) results are in quantitative agreement with exact results obtained for half-filled Hubbard chains from the Bethe-ansatz solution.[29] It is interesting to notice that whereas f_{CT} increases with φ for any U value, b decreases with φ for $U<2.5$ and shows the opposite behavior for $U>2.5$. This seemingly anomalous behavior can be understood by realizing that for small U, electrons are largely delocalized in the undistorted lattice and the chain dimerization localizes them within each dimer. For large U, on the contrary, electrons are strongly localized on the sites and the mean bond order increases with φ since the increased delocalization within each dimer more than compensates the intradimer localization.

In Fig. 5 we report the optical gap (Δ) calculated for different U and φ values. As expected, the optical gap strongly increases with U, and monotonously increases with φ. In general, $\varphi=1$ results are not affected by extrapolation uncertainties: At $\varphi=1$, the chain becomes a collection of noninteracting dimers and the results are size independent. This also holds for Δ, but its value differs from the value relevant to the isolated dimer,

$$\Delta = [U + (U^2+32)^{1/2}]/2 \ .$$

In fact, the lowest electronic excitation does correspond to an interdimer excitation[30] whose energy is calculated at

$$\Delta = (U^2+32)^{1/2} - 2^{3/2} \ ,$$

in agreement with the Fig. 5 data. The calculated gap is in good agreement with previous partial results in Refs. 6 and 14. On the contrary, the variational calculation in Ref. 10 appears to largely underestimate the optical gap.

As suggested by Eqs. (8), $\chi_v^{-1}(\varphi)$and $\chi_b^{-1}(\varphi)$ figures are the phase diagrams for on-site and on-bond charge relaxation. In fact, putting on the ordinate axis the ε_{sp} and ε_d values, stable states are represented by points lying below the curves.[23] Since the calculation of electronic susceptibilities requires the complete diagonalization of the Hamiltonian, the χ_v^{-1} values reported in Fig. 6 are extrapolated from the results obtained for periodic rings up to eight sites and antiperiodic rings up to six sites. The stability of the system with respect to site-CDW distortion strongly increases with U. However, for small U ($U=0,1$), the system becomes more and more stable with respect to site-CDW distortion as the dimerization increases,

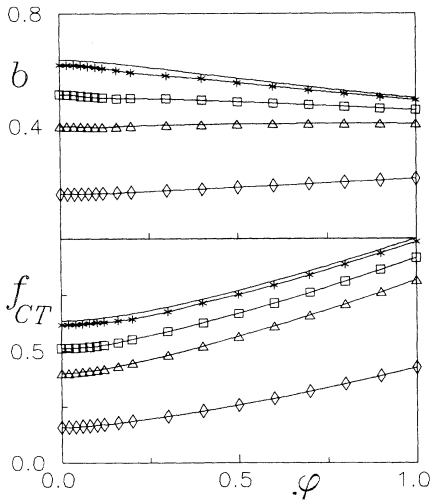

FIG. 4. Top panel: the ground-state bond order b vs φ. Bottom panel: the total oscillator strength f_{CT} vs φ. In both panels, infinite-chain extrapolations are reported. Asterisks, squares, triangles, and diamonds correspond to $U=1$, 2.5, 4, and 12, respectively. The error bars are of the same order as or smaller than the symbols. The solid line (no symbols) refers to the noninteracting case.

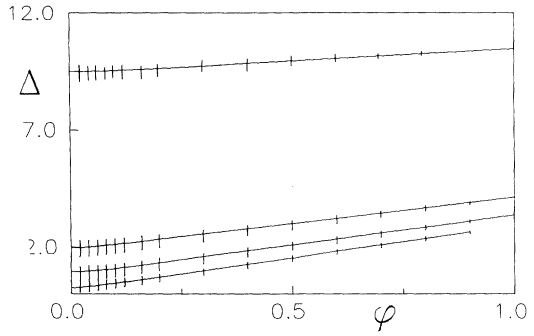

FIG. 5. The optical gap Δ as a function of φ. From top to bottom the curves refer to $U=12$, 4, 2.5, and 1.

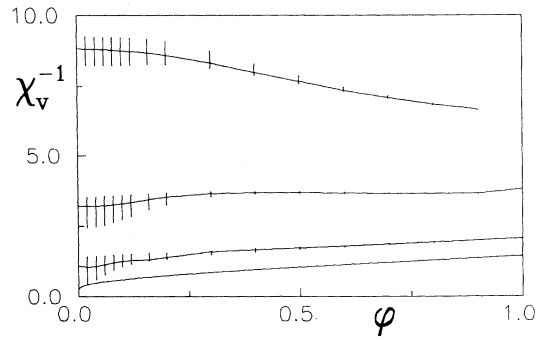

FIG. 6. The inverse of the electronic response to site-diagonal e-ph perturbation, χ_v^{-1}, as a function of φ. From top to bottom the curves refer to $U=4$, 2.5, 1, and 0, respectively.

whereas for large U ($U \geq 2.5$), the stability of the system decreases with φ (the $U=12$ curve, outside the figure range, also has a negative slope). The opposite slope of the $\chi_v^{-1}(\varphi)$ curves at low and high U has the same physical origin as the analogous behavior observed for the $b(\varphi)$ curves. At small U, electrons are largely delocalized along the chain and are therefore highly responsive to site-CDW distortion; by increasing φ, they localize within the dimers and become stiffer. On the contrary, at large U, electrons are strongly localized and dimerization delocalizes them within each dimer, making the system more responsive to site-diagonal e-ph perturbation.

Equation (7) allows us to calculate χ_b also for ten-site periodic rings and eight-site antiperiodic rings, without the need for complete diagonalization. In Fig. 7 we report the $\chi_b^{-1}(\varphi)$ curves calculated for finite-size rings with several U values, together with the analytical $U=0$ results. As in the case of Δ, the χ_b^{-1} values calculated for $\varphi=1$ are different from the values relevant to the isolated dimer ($\chi_b=(\Gamma/4)[32+U(U-\Gamma)^2]/[32-(U-\Gamma)^2]$, with $\Gamma^2=U^2+32$, i.e., $\chi_b^{-1}=\infty$, 47.39, 9.462, 5.196, and 4.054 for $U=0$, 1, 2.5, 4, and 12, respectively), suggesting a large contribution to χ_b from interdimer excitations. However, something very peculiar occurs in this case: Whereas at $\varphi=1$ all the other computed quantities are strictly independent of N and of boundary conditions, χ_b is strongly N dependent, suggesting a contribution from long-range excitations. In fact, χ_b is the sum, with alternating signs, of bond-bond polarizabilities,[31] and nonlocal contributions are expected to be important particularly for small U values (notice that in Fig. 7 the $U=0$ curve relevant to the four-site periodic ring is not shown as $\chi_b^{-1}=\infty$ in this case). Due to the large N dependence of χ_b, the usual extrapolation procedure has been slightly modified. In particular, the extrapolated χ_b^{-1} values reported in Fig. 7 and, with the corresponding uncertainties, in Fig. 8 are obtained as described at the end of Sec. I, but with the exponents of the interpolating polynomials ranging from 1 to 8.

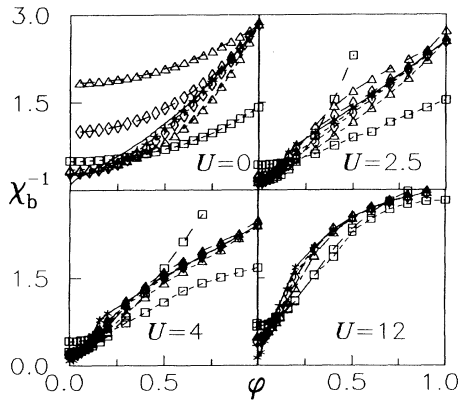

FIG. 7. The inverse of the electronic response to bond-diagonal e-ph perturbation (χ_b^{-1}) vs φ for finite-size rings. Squares, triangles, diamonds, and stars refer to four, six, eight, and ten sites, respectively. Long- and short-dashed lines join points relevant to MPBC and MABC, respectively; the solid lines correspond to the $N=\infty$ extrapolations for finite U and to the analytical result for $U=0$.

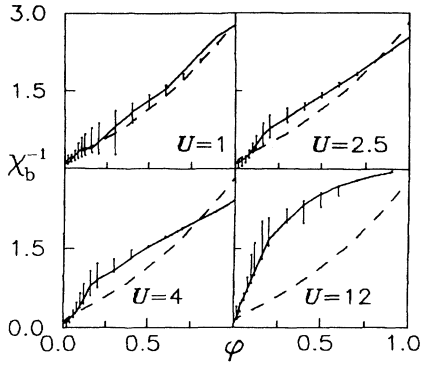

FIG. 8. The inverse of the electronic response to bond-diagonal e-ph perturbation (χ_b^{-1}) vs φ: infinite-chain extrapolations. The dashed lines refer to the noninteracting case.

In the Herzberg-Teller approach,[24] χ_b is directly related to the screening of the phonon frequency. If only one mode is coupled to the electron, its frequency (Ω) is given by

$$\frac{\omega^2-\Omega^2}{\omega^2}=\varepsilon_d\chi_b \ , \tag{9}$$

where ω is the phonon frequency in the absence of e-ph perturbation. As for many other properties, the screening of the phonon frequency shows a nonmonotonous behavior at small ε_d values. As shown in Fig. 9, it first decreases with increasing U and then increases. On the contrary, for large ε_d, the screening increases with U. Our results are in qualitative agreement with the result reported in Ref. 32 for $\varphi=0.1$, but are not in agreement with the variational results in Ref. 10, and in fact for $U=2.5$, we calculate much larger screening. Moreover, an overall increase of the screening with ε_d is only observed in the high U ($U>4$) and high ε_d ($\varepsilon_d>0.5$) regions.

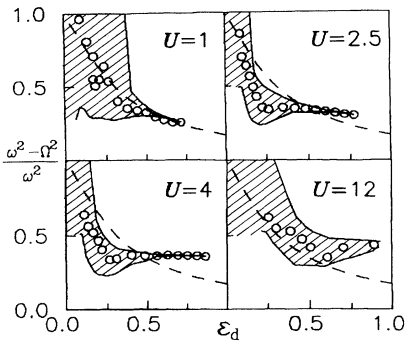

FIG. 9. Screening of the bond-diagonal phonon frequency as a function of the strength of bond-diagonal e-ph coupling (ε_d). The hatched regions correspond to the uncertainties in the extrapolated results (circles) for finite U. The dashed lines refer to the noninteracting case.

IV. THE EFFECT OF INTERSITE *e-e* INTERACTIONS

Figure 10 shows the $\beta(\varphi)$ curves calculated for $U=4$ and several ε_c values. For not too large ε_c, increasing intersite *e-e* interactions have an effect similar to that of decreasing U (cf. Fig. 2), favoring dimerization in the low-φ region.[33] On the contrary, large intersite *e-e* interactions ($V\alpha \gg U$) strongly suppress dimerization. The $\beta(\varphi)$ curves reported in Fig. 10 are transformed with the help of Eq. (5) into the $\beta(\varphi)$ curves reported in Fig. 11 (the $\varepsilon_c=2.23$ curve is not reported in the figure since in this case appreciable dimerization is observed only for $\varepsilon_d \gg 1$). For $V\alpha$ values of the order of or slightly larger than U ($\varepsilon_c=1\div1.23$), a large increase of the bond-CDW amplitude is observed in a wide ε_d range, in good agreement with recent results.[6,12] It is interesting to notice that dimerization is largely favored in the $U\simeq V\alpha$ region, i.e., the region where in the absence of *e*-ph coupling the site-CDW–bond-CDW interface is expected.[12,19] This is not surprising since at the interface electrons are largely delocalized (several states with different electronic distributions have similar energies) and are therefore highly responsive to *e*-ph perturbation.

The charge delocalization at $U\cong V\alpha$ is also clearly pointed out by the $b(\varphi)$ curves reported in Fig. 12. The bond order increases with ε_c, reaching the maximum at $\varepsilon_c=1.11-1.23$ (see the inset in Fig. 12) with approximately the same values as in the noninteracting case (cf. Fig. 4). For $V\alpha \gg U$ ($\varepsilon_c=2.23$), b drops to very small values. Moreover, for both $\varepsilon_c=0$ and 2.23, b slightly increases with φ, suggesting that the electrons, largely localized on the sites, are delocalized within the dimers with increasing dimerization. On the contrary, at intermediate ε_c values, b decreases with φ, indicating that dimerization localizes within the dimers the highly delocalized electrons of the regular chain.

The optical gap Δ, reported in Fig. 13 for $U=4$ and different ε_c, monotonously decreases with ε_c (the $\varepsilon_c=2.23$ curve, not reported in Fig. 12, actually lies on the x axis). The lowering of the optical gap is obviously related to the increased instability of the system with respect to site-CDW distortion, as indicated by the $\chi_v^{-1}(\varphi)$ curves reported in Fig. 14 (notice that for $\varepsilon_c=2.23$, the curve lies on the x axis, i.e., the system is unstable with respect to site-CDW formation even in the absence of site-diagonal *e*-ph coupling). As already observed for Fig. 6, systems with largely localized electrons

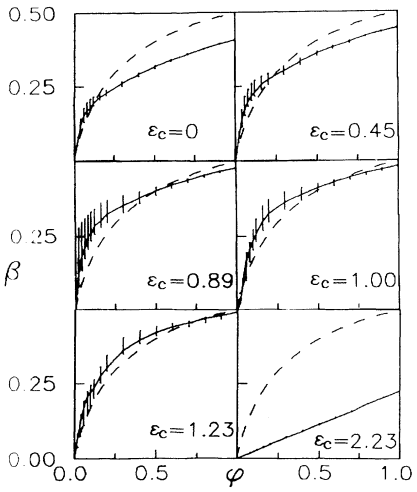

FIG. 10. The bond-CDW amplitude β as a function of φ for the infinite chain with $U=4$ and several ε_c values. The dashed lines refer to the noninteracting case.

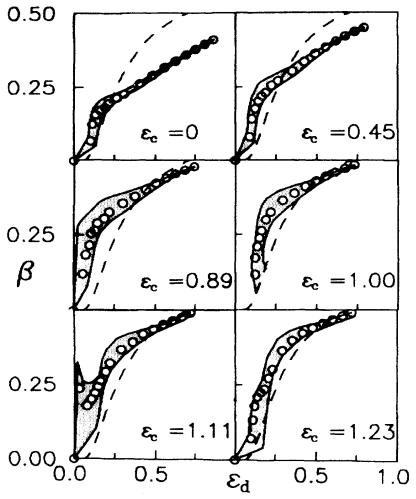

FIG. 11. The bond-CDW amplitude β as a function of the strength of bond-diagonal *e*-ph coupling (ε_d) for the infinite chain with $U=4$ and several ε_c values. The shaded regions correspond to the uncertainties in the extrapolated results (circles). The dashed lines refer to the noninteracting case.

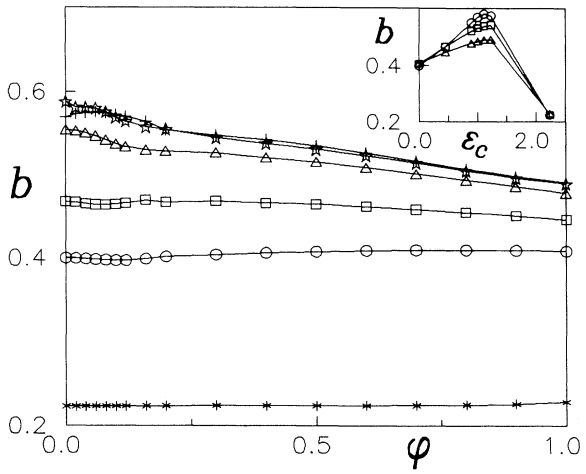

FIG. 12. The ground-state bond order b as a function of φ, calculated for the infinite chain with $U=4$ and several ε_c: circles, squares, triangles, diamonds, stars, pluses, and asterisks refer to $\varepsilon_c=0$, 0.45, 0.89, 1.00, 1.11, 1.23, and 2.23, respectively. The error bars are of the same order as or smaller than the symbols. The inset shows the b dependence on ε_c for $\varphi=0.04$ (circles), 0.4 (squares), and 1.0 (triangles).

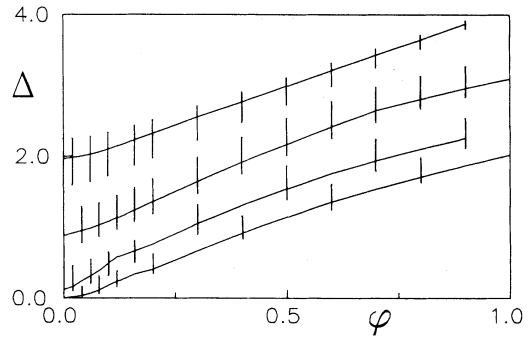

FIG. 13. The optical gap Δ as a function of φ for the infinite chain with $U=4$ and several ε_c. From top to bottom the curves refer to $\varepsilon_c=0$, 0.89, 1.11, and 1.23. The $\varepsilon_c=2.23$ curve lies on the x axis.

(large U-$V\alpha$) become, by increasing φ, more and more unstable with respect to site-CDW distortion (χ_v^{-1} decreases), whereas highly delocalized systems (small U-$V\alpha$) show increased stability.

In Fig. 15 we compare the $\chi_b^{-1}(\varphi)$ curves calculated for $U=4$ and several ε_c values with the $U=0$ curves (dashed lines). In this case, due to large uncertainties in the extrapolated values, we report the results obtained for ten-site periodic rings. Once more, increasing ε_c values up to $\varepsilon_c \cong 1.23$ has an effect similar to that of decreasing U, whereas a qualitatively different result is obtained for $V\alpha \gg U$ ($\varepsilon_c=2.23$).

Before closing this section, we notice that we have neglected the modulation of intersite e-e interactions due to bond-diagonal phonons. Its inclusion makes the calculations more numerically intensive: In fact, charge correlations also have to be calculated in order to extract ε_d from the $\beta(\varphi)$ data.[11] On the other hand, the linear e-ph coupling term arising from the modulation of intersite e-e interactions is expected to give large contributions only in the large-φ region (it actually vanishes at $\varphi=0$). The effect of quadratic (or higher-order) terms, which can also be large in the small dimerization regime,[11] can be

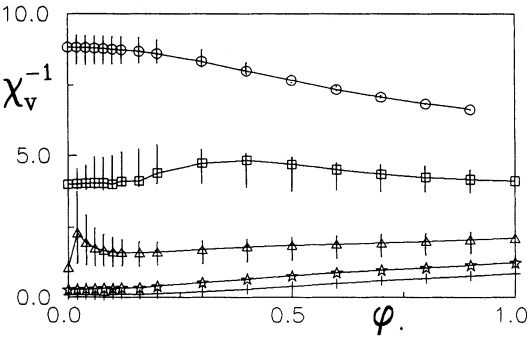

FIG. 14. The inverse of the electronic response to site-diagonal e-ph perturbation (χ_v^{-1}) as a function of φ for the infinite chain with $U=4$ and several ε_c values. Circles, squares, triangles, stars, and pluses refer to $\varepsilon_c=0$, 0.45, 0.89, 1.11, and 1.23, respectively. The $\varepsilon_c=2.23$ curve lies on the x axis.

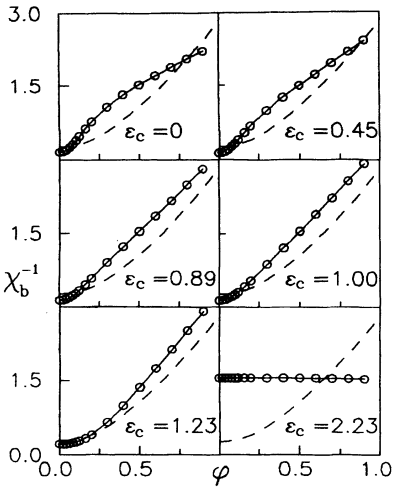

FIG. 15. The inverse of the electronic response to bond-diagonal e-ph perturbation, χ_b^{-1}, as a function of φ, calculated for ten-site periodic rings with $U=4$ and several ε_c. The dashed lines refer to the ten-site periodic ring with no e-e interactions.

conveniently included into the definition of the reference state via a renormalization of the reference phonon frequency (ω).[31]

V. CONCLUSIONS

In this paper we have described the results of DVB calculations performed on a long-range extended Hubbard model with alternating CT integrals. Calculations have been performed on rings up to ten sites, with either periodic or antiperiodic boundary conditions, yielding accurate extrapolations to the infinite-chain limit. We have investigated systems with variable φ and different strengths of on-site and intersite e-e interactions. Apart from the bond-CDW amplitude, we have calculated several properties of the systems, many of them being related to experimentally accessible quantities. The optical gap and the CT oscillator strength are directly measured by the electronic optical spectrum, whereas the screening of the phonon frequency can be extracted by a careful analysis of the vibrational (Raman) spectra.[31]

By assigning the alternation of CT integrals to the relaxation of involved phonons, the present calculations allow us to investigate the bond-CDW regime of a half-filled Hubbard chain in the presence of bond-diagonal e-ph coupling. In particular, we extract from the $\beta(\varphi)$ curve the corresponding strength of bond-diagonal e-ph coupling in such a way that all the computed quantities can be expressed as functions of ε_d.

In a previous paper[19] we have investigated half-filled Hubbard chains in the presence of on-site energy alternation, getting information on the site CDW of a half-filled chain in the presence of site-diagonal e-ph coupling. In a forthcoming paper,[20,22] by collecting the results obtained for the two kinds of relaxed systems, we will be able to construct the phase diagram of a half-filled chain, described in terms of interacting electrons coupled to adiabatic phonons modulating on-site and on-bond energies.

ACKNOWLEDGMENTS

We thank Z. G. Soos and J. Voit for enlightening discussions and correspondence. Thanks are due to J. Tinka Gammel for his critical and accurate reading and useful suggestions. The calculations have been performed at the "Centro di Calcolo Elettronico" in Parma. Financial support from the National Research Council (CNR) and from the Italian Ministry of University and Scientific and Technological Research is acknowledged. This work was developed within the CNR "Progetto Finalizzato Materiali Speciali per Tecnologie Avanzate."

APPENDIX: THE NONINTERACTING ELECTRON CASE

The Hamiltonian [Eq. (1)] with no *e-e* interactions ($U=V_{ij}=0$) has already been solved.[34] The ground-state energy per site is

$$\mathcal{E}=-\frac{(2)^{3/2}}{\pi}E(1-\varphi^2)\ , \tag{A1}$$

where $E(x)$ is the complete elliptic integral of the second type. From the energy all quantities of interest can be evaluated as follows:

$$\beta=-\frac{1}{\sqrt{2}}\frac{\partial\mathcal{E}}{\partial\varphi}=\frac{2\varphi}{\pi}K(\varphi,1,0,1)\ , \tag{A2}$$

where

$$K(k,p,a,b)=\int_0^{\pi/2}d\vartheta\frac{(a\cos^2\vartheta+b\sin^2\vartheta)}{(\cos^2\vartheta+p\sin^2\vartheta)(\cos^2\vartheta+k^2\sin^2\vartheta)^{1/2}} \tag{A3}$$

is the complete elliptic integral as defined in Ref. 35. Moreover,

$$b=-\frac{1}{2}\frac{\partial\mathcal{E}}{\partial t}=\frac{2}{\pi}K(\varphi,1,1,0) \tag{A4}$$

and

$$\chi_b=-2\frac{\partial^2\mathcal{E}}{\partial\varphi^2}=\frac{4\sqrt{2}}{\pi(1-\varphi^2)}K(\varphi,1,-1,1)\ . \tag{A5}$$

To evaluate χ_v, we introduce in the electronic Hamiltonian a term accounting for the alternation of on-site energies:

$$\mathcal{H}_\Delta=-\frac{\Delta}{2}\sum_{i,\sigma}(-1)^i a_{i,\sigma}^\dagger a_{i,\sigma}\ . \tag{A6}$$

The ground state energy is[36]

$$\mathcal{E}=-\frac{1}{\pi}\int_{-\pi/2}^{\pi/2}d\vartheta\left[\frac{\Delta^2}{4}+2\varphi^2\sin^2\vartheta+2\cos^2\vartheta\right] \tag{A7}$$

and

$$\chi_v=-4\frac{\partial^2\mathcal{E}}{\partial\Delta^2}=\frac{\sqrt{2}}{\pi}K(\varphi,1,1,1)\ . \tag{A8}$$

[1] Z. G. Soos and G. W. Hayden, in *Electroresponsive and Polymeric Systems,* edited by T. A. Skotheim (Marcel Dekker, New York, 1988), p. 197, and references therein.

[2] D. Baeriswyl, D. K. Campbell, and S. Mazumdar, in *Conjugated Conducting Polymers,* edited by H. Kiess (Springer-Verlag, New York, 1992), p. 7, and references therein.

[3] P. Horsch, Phys. Rev. B **24**, 7351 (1981).

[4] S. Kivelson and D. E. Heim, Phys. Rev. B **26**, 4278 (1982).

[5] S. Mazumdar and S. N. Dixit, Phys. Rev. Lett. **51**, 292 (1983); S. N. Dixit and S. Mazumdar, Phys. Rev. B **29**, 1824 (1984).

[6] J. E. Hirsch, Phys. Rev. Lett. **51**, 296 (1983).

[7] D. K. Campbell, T. A. DeGrand, and S. Mazumdar, Phys. Rev. Lett. **52**, 1717 (1984); J. Stat. Phys. **43**, 803 (1986).

[8] Z. G. Soos and S. Ramasesha, Phys. Rev. B **29**, 5410 (1984).

[9] G. W. Hayden and E. J. Mele, Phys. Rev. B **32**, 6527 (1985); **34**, 5484 (1986).

[10] D. Baeriswyl and K. Maki, Phys. Rev. B **31**, 6633 (1985); Synth. Met. **17**, 13 (1987); E. Jeckelmann, D. Baeriswyl, and X. Zotos, *ibid.* **57**, 4249 (1993).

[11] G. W. Hayden, and Z. G. Soos, Phys. Rev. B **38**, 6075 (1988).

[12] V. Waas, J. Voit, and H. Büttner, Synth. Met. **27**, 21 (1988); V. Waas, H. Büttner, and J. Voit, Phys. Rev. B **41**, 9366 (1990).

[13] V. A. Kuprievich, Phys. Rev. B **40**, 3882 (1989).

[14] E. Y. Loh, D. K. Campbell, and J. T. Gammel, in *Interacting Electrons in Reduced Dimensions,* Vol. 213 of *NATO Advanced Study Institute, Series B: Physics,* edited by D. Baeriswyl and D. K. Campbell (Plenum, New York, 1989), p. 91; E. Y. Loh and D. K. Campbell, Synth. Met. **27**, A499 (1988).

[15] G. König and G. Stollhoff, Phys. Rev. Lett. **65**, 1239 (1990).

[16] A. Girlando, A. Painelli, and C. Pecile, Mol. Cryst. Liq. Cryst. **171**, 69 (1989), and references therein.

[17] A. Painelli nd A. Girlando, Synth. Met. **29**, F181 (1989).

[18] A. Painelli and A. Girlando, in *Interacting Electrons in Reduced Dimensions* (Ref. 14), p. 189.

[19] A. Painelli and A. Girlando, Phys. Rev. B **45**, 8913 (1992).

[20] A. Painelli and A. Girlando, Synth. Met. **57**, 4543 (1993).

[21] S. Ramasesha and Z. G. Soos, J. Chem. Phys. **80**, 3278 (1984); Int. J. Quantum Chem. **25**, 1003 (1984). See also Z. G. Soos and S. Ramasesha, in *Valence Bond Theory and Chemical Structure,* edited by D. J. Klein and N. Trinajstic (Elsevier, Amsterdam, 1990), p. 81.

[22] A. Painelli and A. Girlando (unpublished).

[23] A. Painelli and A. Girlando, Phys. Rev. B **37**, 5748 (1988); **39**, 9663(E) (1989).

[24] A. Painelli and A. Girlando, J. Chem. Phys. **84**, 5655 (1986).

[25] P. R. Bevington, *Data Reduction and Error Analysis for the Physical Sciences* (McGraw-Hill, New York, 1960), p. 235.

[26] A. Painelli and A. Girlando, J. Chem. Phys. **87**, 1705 (1987).

[27] R. M. Fye *et al.,* Phys. Rev. B **44**, 6909 (1991).

[28] J. T. Gammel *et al.,* Synth. Met. **43**, 3471 (1991).

[29] D. Baeriswyl, J. Carmelo, and A. Luther, Phys. Rev. B **33**, 7247 (1986).

[30] M. Meneghetti, Phys. Rev. B **44**, 8554 (1991).

[31] A. Girlando, A. Painelli, and Z. G. Soos, Chem. Phys. Lett. **198**, 9 (1992); A. Girlando, A. Painelli, and Z. G. Soos, J. Chem. Phys. **98**, 7459 (1993).

[32] D. K. Campbell, J. T. Gammel, and E. Y. Loh, Phys. Rev. B **42**, 475 (1990).

[33]S. Mazumdar and D. K. Campbell, Phys. Rev. Lett. **55**, 2067 (1985).

[34]W. P. Su, J. R. Schrieffer, and A. J. Heeger, Phys. Rev. B **22**, 2099 (1980).

[35]W. H. Press, B. P. Flannery, S. A. Teukolsky, and W. T. Vetterling, *Numerical Recipes* (Cambridge University Press, New York, 1987), Chap. 6.

[36]M. J. Rice and E. J. Mele, Phys. Rev. Lett. **49**, 1455 (1982).